Available online at www.sciencedirect.com

ScienceDirect

journal homepage: www.elsevier.com/locate/he

Development and performance of iron based oxygen carriers containing calcium ferrites for chemical looping combustion and production of hydrogen

Mohammad Ismail [a,*], *Wen Liu* [b], *Matthew T. Dunstan* [c], *Stuart A. Scott* [a]

[a] *Department of Engineering, University of Cambridge, Cambridge, CB2 1PZ, UK*
[b] *Cambridge Centre for Advanced Research in Energy Efficiency in Singapore, Nanyang Technological University, Singapore 637459*
[c] *Department of Chemistry, University of Cambridge, Cambridge, CB2 1EW, UK*

ARTICLE INFO

Article history:
Received 11 August 2015
Received in revised form
12 November 2015
Accepted 13 November 2015
Available online 29 January 2016

Keywords:
Chemical looping combustion
Chemical looping hydrogen production
Carbon dioxide capture
Fluidised bed
Calcium ferrites

ABSTRACT

Chemical looping combustion (CLC) is a cyclic process in which an oxygen carrier (OC), is firstly reduced by a fuel, *e.g.* syngas, and then oxidised in air to produce heat. If the OC is Fe_2O_3, the oxidation can take place in steam to produce hydrogen, i.e. chemical looping hydrogen production (CLH). This paper presents an investigation of CaO modified Fe_2O_3 OCs for CLC and CLH. The performance of the mechanically mixed OCs were examined in a thermogravimetric analyser and a fluidised bed. It was found that the addition of CaO gives cyclic stability and additional capacity to produce hydrogen via CLH, at the expense of reduced oxygen carrying capacity for CLC, owing to the formation of calcium ferrites, such as $Ca_2Fe_2O_5$.

Introduction

Chemical looping combustion (CLC) combusts fuels using reduction–oxidation cycles of oxygen carriers to keep the products of combustion separate from the air used for combustion [1]. In some cases the oxygen carrier can directly release gas phase oxygen, leading to the chemical looping with oxygen uncoupling process (CLOU) [2]. The oxygen-carrier requires sufficient and stable oxygen transport capacity over many cycles of oxidation and reduction. Oxides of Ni, Fe, Cu, Mn and Co are popular candidates for oxygen carriers for use in CLC [3]. Fe_2O_3 is cheap, widely available and environmentally benign and has been used in a number of studies [4–7]. The equilibria for the phase transitions for the Fe–O system are such that only the reduction of Fe_2O_3 to Fe_3O_4 will result in complete oxidation of a fuel [8]. The subsequent reductions to Fe_xO (i.e. wüstite where x ~0.95 and can vary) and

* *Corresponding author*. Energy Laboratory, ISO-45, Department of Engineering, University of Cambridge, Trumpington Street, Cambridge, CB2 1PZ, UK. Tel.: +44 7841419325; fax: +44 1223765311.
E-mail address: mi286@cam.ac.uk (M. Ismail).
http://dx.doi.org/10.1016/j.ijhydene.2015.11.066

Fe, are also usually found to be much slower [9]. Chemical looping hydrogen (CLH) production [10] (also known as the cyclic-water gas shift [11] or the steam iron process [12–15]) uses steam during the oxidation stage to produce H_2. Whether a phase transition can be used to produce H_2 depends on the equilibrium oxygen partial pressure (p_{O_2}); reactions with p_{O_2} suitable for near complete combustion to H_2O cannot easily be reversed to produce H_2. The oxidation of Fe and, or Fe_xO to Fe_3O_4 by steam can produce H_2 [8,16,17]. The stoichiometry is such that the oxidation of iron to Fe_3O_4 produces approximately four-times more H_2 than that for Fe_xO to Fe_3O_4.

Unsupported metal oxides usually agglomerate, or lose their ability to transfer oxygen over many cycles [8,18,19]. Granulated Fe_2O_3 was found to be stable over repeated cycles of conversion between Fe_2O_3 to Fe_3O_4 and Fe_2O_3 to Fe_xO, but deactivated when reduced to Fe [8]. Thus, it is common to mix the iron oxide with support materials either to improve kinetics, or to improve the cyclic stability; *e.g.* Fe_2O_3 on $MgAl_2O_4$ [20,21], Fe_2O_3 on Al_2O_3 [22,23], various refractory (oxides of Mg, Al, Cr, Si etc.) dopants impregnated into granulated iron [24] or added during co-precipitation from metal nitrates [14]. Previous studies have shown that Fe_2O_3 supported on Al_2O_3 improved stability [22,23]. In contrast, a SiO_2 support resulted in the formation of undesirable Fe_2SiO_4, which is unreactive under chemical looping conditions [21]. Iron oxide supported on $Ce_{0.5}Zr_{0.5}O_2$ [11,25] or with ZrO_2 [26] has been shown to be stable over many cycles. Support materials can also interact in ways which alter the redox chemistry, *e.g.* Al_2O_3 forms various solid solutions with iron oxide and $FeAl_2O_4$ during reduction [27,28]. $FeTiO_3$ ore has been suggested as a cheap oxygen carrier [29], in which the iron oxide is already supported by the titania. During chemical looping $FeTiO_3$ oxidises to Fe_2TiO_5, and also segregates to give free iron oxide [30]; the material is often observed to become more reactive after a few cycles. For H_2 production, the $FeTiO_3$ must be reduced to metallic Fe; the kinetics of which have been found to be faster than those for reduction of wüstite; density functional theory calculations suggested that diffusion of O^{2-} through the $FeTiO_3$ lattice facilitates reduction [31].

Oxygen carriers consisting of two active metal oxides have also been reported [32,33]. For CLOU combustion, in which the oxygen carrier releases gas phase oxygen, the iron + manganese oxide system has been proposed, with the mixed oxide phase showing favourable oxygen release equilibrium compared to Fe_2O_3 or Mn_2O_3 alone [2]. Svoboda et al. [32] suggested $NiFe_2O_4$ and $CoFe_2O_4$ as potential materials for CLH based on a thermodynamic feasibility study. They also suggested that additional H_2 (per mole of Fe) can be produced if the reduced OCs are re-oxidised to spinel phases (*e.g.* $NiFe_2O_4$ or $CoFe_2O_4$) because the formation of spinels allows oxidation of more Fe^{2+} to Fe^{3+}. In contrast, it is practically impossible to oxidise iron oxide to an oxidation state higher than Fe_3O_4 using steam. Other iron containing materials, based on perovskite structures [10,34] have also been proposed. Perovskite materials can accommodate significant oxygen non-stoichiometry, allowing oxidation or reduction without phase changes, potentially improving cyclic stability [10]. They also allow O^{2-} ion conduction, which should facilitate access to the oxidising or reducing species in the particle whether they are used as the actual looping material themselves [32], or as a support, e.g. in composite oxygen carriers [35].

Thus, the support can interact with the active metal oxide in several ways, either by forming new phases with different redox equilibria (e.g. Fe–Mn carriers [2]), segregating or forming new phases during cycling (e.g. TiO_2 [30], Al_2O_3 [27,28]), providing porosity and separation between active metal grains, providing paths for ionic conduction (e.g. ZrO_2 [26] or perovskites [35]), or altering the transport of ions within crystals by introducing defects or oxygen vacancies [36], either in the support or the active metal oxide phase.

The objective of this study is to investigate calcium oxide as the support material for Fe_2O_3. CaO, like Fe_2O_3, is cheap and environmentally benign and the thermodynamics of the Ca–Fe–O system is well known [37]. Calcium and iron oxide form a variety of calcium ferrite phases, with reduction/oxidation equilibria which differ from those of pure iron oxides. One such ferrite, $Ca_2Fe_2O_5$ (i.e. a brownmillerite-type ferrite), has received particular attention owing to its structure which facilitates fast oxygen ion transport [38], leading to its use as a fuel cell cathode [39] or as a membrane material. At temperatures lower than those used for CLC some of the Fe can take on the +4 oxidation state within the brownmillerite structure, leading to very active oxygen species which can be used to catalyse combustion [40]. $Ca_2Fe_2O_5$ has also been suggested as catalyst for oxidation of CO, NH_3 and hydrocarbons [41].

Thermodynamics

When CaO is added to Fe_2O_3 various phases can form at equilibrium, depending on the equilibrium oxygen partial pressure (which is related to the ratio of CO_2 to CO, or H_2O to H_2 at equilibrium), temperature, and composition. Fig. 1 (calculated using MTDATA with the NPL oxide database [42]) shows the calculated phase boundaries for the Fe–Ca–O system at 1173 K. Various ferrite phases can form and are denoted as combinations of sub-lattice species with: C = CaO, F = Fe_2O_3, W = FeO; e.g., CF = $CaFe_2O_4$ ($CaO.Fe_2O_3$) and C_2F = $Ca_2Fe_2O_5$ ($2CaO.Fe_2O_3$). The form of the phase diagrams for other temperatures used are effectively the same, though with differing values of p_{O_2} for the phase transitions and with the region labelled as "C_2F + FeO" disappearing below 1143 K.

Experimental

Synthesis of oxygen carriers

Wet-granulated particles of unsupported iron oxide were prepared by spraying water into iron oxide powders (99 wt%, Sigma-Aldrich), while stirring the mixture. The resulting agglomerates were sieved to give 425–500 μm particles and then sintered at 1273 K for 6 h and re-sieved. Particles with different ratios of Fe_2O_3 to CaO (50, 57.3 and 66.7 mol% CaO) were prepared by mechanical mixing. Measured amounts of iron oxide and calcined CaO (97+%, Acros Organics) powders were mixed with a small amount of ethanol (99.8+%, Fisher Scientific) (to aid mixing) and ball milled (SFM-1, MTI Corporation) for 3 h at

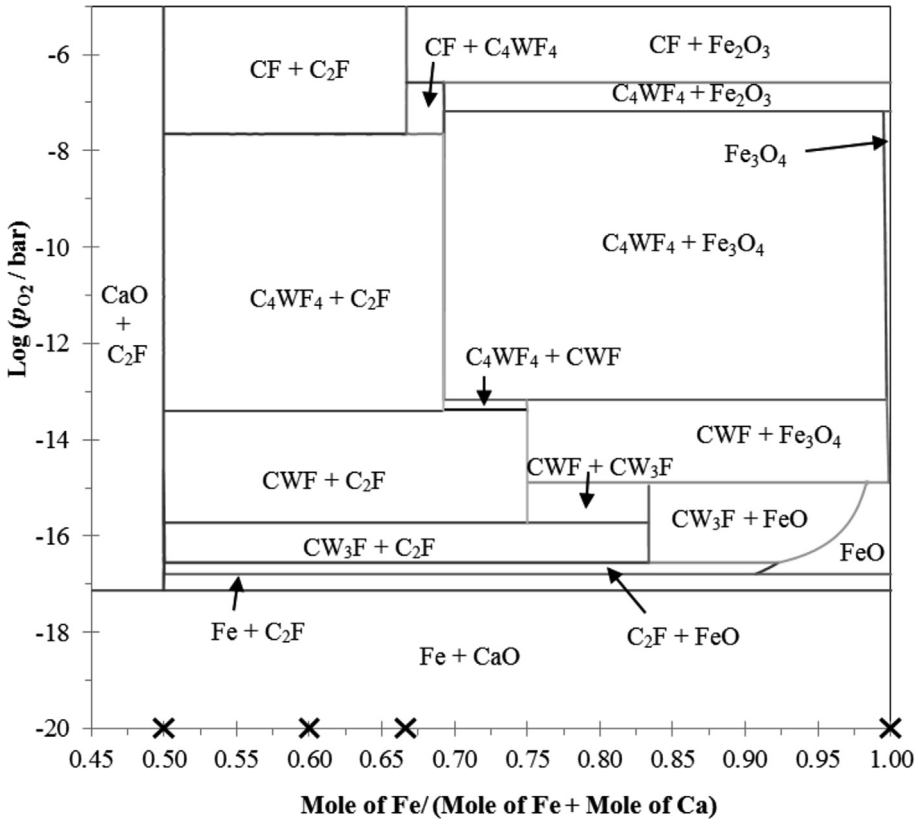

Fig. 1 – An oxygen potential vs composition phase diagram of the Ca–Fe–O system at 1173 K calculated using MTDATA [42]. ' × ' denotes the compositions of the oxygen carriers investigated here.

1560 rpm. The milled material was then calcined at 1273 K for 6 h, crushed and sieved to recover 425–500 μm particles. Henceforth, the oxygen carriers are denoted by the mole fraction of CaO they contain if no ferrite forms i.e. FC0, FC50, FC57 and FC67.

Thermogravimetric analysis (TGA)

A thermogravimetric analyser (TGA/DSC 1, Mettler Toledo) was used to perform redox cycles and temperature programmed reduction (TPR). In all TGA experiments, a permanent flow of N_2 gas (zero grade, BOC) was used as protective gas and purge gas, both at a flow rate of 50 ml/min (at 293 K and 1 atm.). A reactive gas, either air (BOC standard grade) or 5% H_2 in N_2, (spectra shield, BOC) was fed to the reactive gas port at a rate of 50 ml/min as required. Between oxidising and reducing stages the line was purged with N_2.

In a TPR (Temperature-programmed reduction) experiment, ~30 mg of oxygen carrier was first heated in air to 1273 K at 10 K/min and held there for 10 min to remove contamination, then cooled to 473 K. The particles were then heated to 1323 K at a rate of 5 K/min, in 5 vol% H_2/N_2, and held for 2 h.

In a cycling experiment, 25–30 mg of the oxygen carrier particles were heated to 1173 K with air as the reactive gas. The oxygen carrier was then exposed to alternating reducing and oxidising conditions using 5 vol% H_2 in N_2 or air as the reactive gas. Some experiments were also performed with the H_2/N_2 replaced by a mixture of 50 vol% CO_2 + 5 vol% CO in N_2.

During reduction, the conversion of the metal oxide is taken to be $X_{red} = (m_o - m)/\Delta m_{max}$, where m is the mass of sample, m_o is the mass of the fully oxidised sample and Δm_{max} is the mass change expected if all of the Fe^{3+} in the sample is reduced to metallic Fe. During oxidation, the conversion is defined here as $X_{ox} = 1 - X_{red}$. The change in conversion ΔX_{red} and ΔX_{ox} during reduction and oxidation, respectively, then give a measure of the oxygen transferred during a cycle.

Cyclic performance of oxygen carriers in a fluidised bed

A graphical representation of the fluidised bed reactor system is shown in Fig. 2. The reactor tube was made of re-crystallised Al_2O_3 (Almath Crucibles Ltd., i.d. 19.5 mm). The distributor consisted of a 22 mm thick layer of Al_2O_3 sand (d_p ~ 2 mm), fixed in place by cement (AL/CS, Fortafix). During a typical experiment, a 20 ml bed of recrystallized Al_2O_3 sand (d_p ~ 400 μm), is electrically heated to the required temperature, while fluidised by N_2 at a flow rate 1.8 L/min (at 293 K and 1 atm). Then, 1.0 g of oxygen carrier (sieved to 425–500 μm) was added to the hot bed. Flowrates of the inlet gases were measured and controlled using calibrated rotameters and gas-switching was achieved using computer controlled solenoid valves. The nominal flowrate of the fluidising gas was maintained at 1.8 L/min (as measured at 293 K and 1 atm), which corresponds to the U/U_{mf}, ≈ 7, where U is the superficial velocity of the fluidising gas and U_{mf} is the minimum fluidisation velocity (calculated using Wen and Yu's correlation [43]). The effluent gas was sampled at a rate of 0.5 L/min, through glass

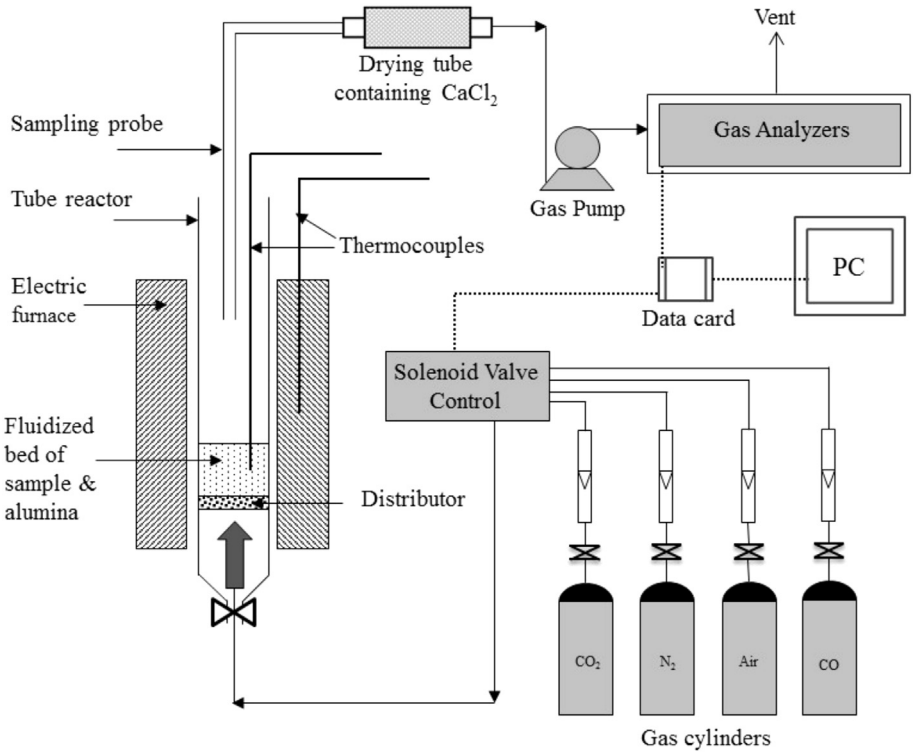

Fig. 2 – Schematic diagram of the fluidised bed reactor system.

wool and a drying tube (containing $CaCl_2$), before analysis by an infrared gas analyser (Uras26, EL3020, ABB), which measures [CO] and [CO_2]. Samples of the solids for analysis were recovered rapidly from the bed and cooled in a flow of 2.0 L/min of N_2.

During the cycling experiments, the fluidising gas was, in turn: (i) N_2 (purge, 2 min), (ii) 10 vol% CO in N_2 (13 min), (iii) N_2 (2 min), (iv) 20 vol% CO_2 in N_2 (13 min), (v) N_2 (purge, 2 min), and (vi) air (to complete oxidation, 8 min). The moles of CO_2 produced during reduction by CO, N_{CO_2}, and the amount of CO produced during oxidation by CO_2 (which is an analogue of H_2 production), N_{CO}, were calculated from the measured mole fractions, y_{CO}, y_{CO_2} and the total molar flow, N_T, using $N_{CO_2} = N_T \times \int y_{CO_2} dt$ and $N_{CO} = N_T \times \int y_{CO} dt$, respectively.

Characterisation of oxygen carriers

Powder X-ray diffraction (XRD) was performed to detect the presence of possible phases in the solid samples. The XRD patterns were collected using a Panalytical Empyrean diffractometer with Cu Kα radiation. Preliminary phase identification was performed using the Panalytical X'Pert High Score Plus software, and the exact phase composition was subsequently determined by Rietveld refinement using GSAS with the graphical interface EXPGUI [44,45].

The surface morphology of the fresh and reacted samples was studied using a scanning electron microscope (JEOL-5800LV). The solid samples were sputter-coated with a thin layer of platinum prior to the SEM analysis. The BET surface area [46] of the prepared samples was determined by N_2 adsorption at 77 K (TRISTAR 3000, Micromeritics).

Results

Characterisation of the as-prepared materials

Fig. 3 shows the XRD patterns of the freshly prepared samples; all of the peaks in Fig. 3 can be indexed by $CaFe_2O_4$, $Ca_2Fe_2O_5$, Fe_2O_3, and CaO phases. From Fig. 1, assuming equilibrium, mono-calcium ferrite ($CaFe_2O_4$ = CF) and/or di-calcium ferrite ($Ca_2Fe_2O_5$ = C_2F) should be present after calcination in air.

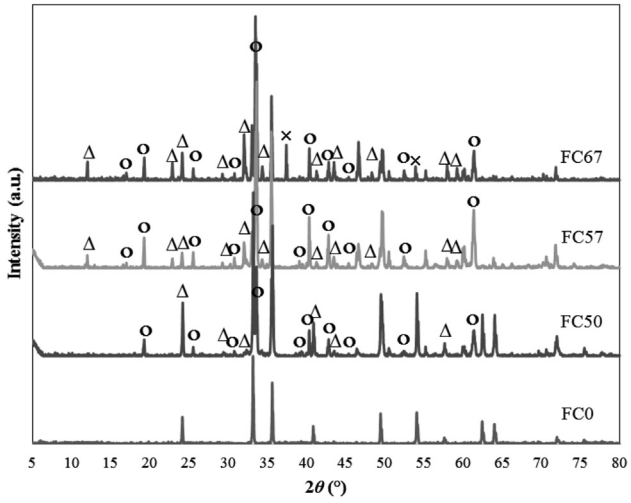

Fig. 3 – XRD patterns of fresh FC0, FC50, FC57 and FC67. Selected peaks are labelled by: O ($CaFe_2O_4$), Δ ($Ca_2Fe_2O_5$), × (CaO).

Table 1 – Comparison of phases predicted by thermodynamic calculations and those identified in XRD and calculated using Rietveld refinement, for the freshly prepared OCs.

Oxygen carrier	Phase composition at equilibrium	Phases composition detected by XRD and fractionated by rietveld refinements
FC50	$CaFe_2O_4$ (100 wt%)	$CaFe_2O_4$ (85 wt%), Fe_2O_3 (15 wt%)
FC57	$CaFe_2O_4$ (60 wt%) & $Ca_2Fe_2O_5$ (40 wt%)	$CaFe_2O_4$ (66 wt%), $Ca_2Fe_2O_5$ (34 wt%)
FC67	$Ca_2Fe_2O_5$ (100 wt%)	$CaFe_2O_4$ (40 wt%), CaO (4 wt%), $Ca_2Fe_2O_5$ (56 wt%)

Table 1 compares the expected compositions (i.e. those computed if at equilibrium as in Fig. 1) with those obtained by Rietveld refinement of the XRD pattern in Fig. 3; given the quality of the XRD patterns, the refinement should be regarded as approximate (e.g. perhaps missing some phases which are present at a levels below the detection limit), but does clearly show that synthesised oxygen carriers have not reached equilibrium, with FC57 being the closest to equilibrium. This is probably because of imperfect mixing between the CaO and Fe_2O_3, and slow solid state diffusion during calcination.

Fig. 4 shows the mass loss and the normalised rate of mass change, ($dm/dt/m_o$), as functions of temperature during TPR with H_2. Based on the final conversions achieved in Fig. 4(a), the iron content is in agreement with that expected from the nominal composition, i.e. 53, 42.5 and 33.5 mol% inferred from the mass loss for FC50 (50 mol% Fe_2O_3), FC57 (42.7 mol% Fe_2O_3), FC67 (33.3 mol% Fe_2O_3), respectively. For FC0, three stages of reaction can been seen in the differential of mass change (DTG) curve in Fig. 4(b): the first peak between733 K and 873 K can be attributed to the reduction of Fe_2O_3 to Fe_3O_4; the second broad peak to the reduction of Fe_3O_4 to Fe_xO (up to ~1073 K); the final peak to reduction to iron. However, the samples containing calcium ferrites show very different profiles of TPR, as a result of the reduction and formation of various ferrites. From the overall mass change, it can be inferred that any ferrites which do form are reducible in H_2.

Performance in redox cycling in the fluidised bed

Fig. 5 shows a typical concentration profile during the cycling of FC57 in the fluidised bed. The times used for reduction and oxidation were based on a preliminary observation that after about 13 min, the reduction of FC0 became very slow after reaching a conversion of $X_{red} = 0.88$, implying it had reduced mostly to iron with some wüstite. The amount of CO_2 produced during reduction of fixed duration in a cycle is an indirect way of comparing how the kinetics of the reactions change with cycling.

Fig. 6(a) shows the amount of CO_2 produced during the reduction phase for 20 cycles. In the case of FC0, 88% of the theoretical solid conversion was obtained in the 1st cycle, but the yield, defined as mmol of CO/CO_2 produced (oxygen atoms transferred) per g of oxygen carrier, reduced drastically from the 2nd cycle. Bohn et al. [8] also found that unmodified iron oxide particles quickly deactivated when reduced to iron. In contrast, the Ca-containing oxygen carriers yielded less CO_2 per gram in the first cycle, but more in the subsequent cycles than pure Fe_2O_3, with more stable yields. To simulate H_2 production (and to avoid the complication with feeding steam) the reduced OCs were oxidised using CO_2, which has an oxidising potential similar to that of steam at 1123 K, to achieve oxidation of Fe and FeO to Fe_3O_4 [47,48].

Fig. 6(b) shows that the yield of CO during oxidation with CO_2 follows the same patterns as that seen in Fig. 6(a). Fig. 7 (for FC57) shows that the stability over cycles is also maintained at 1173 K, however, there appears to be some degradation in the oxygen transfer capacity at 1223 K.

Redox cycles in the TGA

The conversion achieved over 50 cycles, which consisted of an 80 min reduction with H_2 and 40 min oxidation with air at

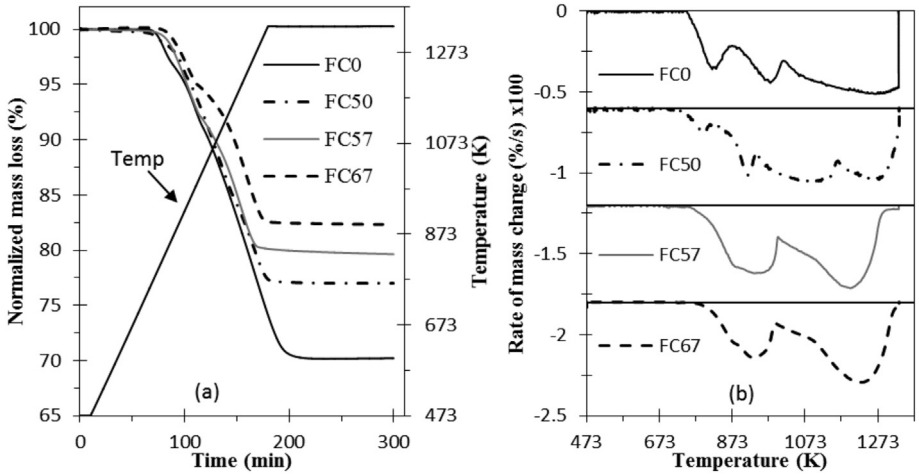

Fig. 4 – (a) Normalised mass loss during TPR and (b) DTG for fresh FC0, FC50, FC57 and FC67.

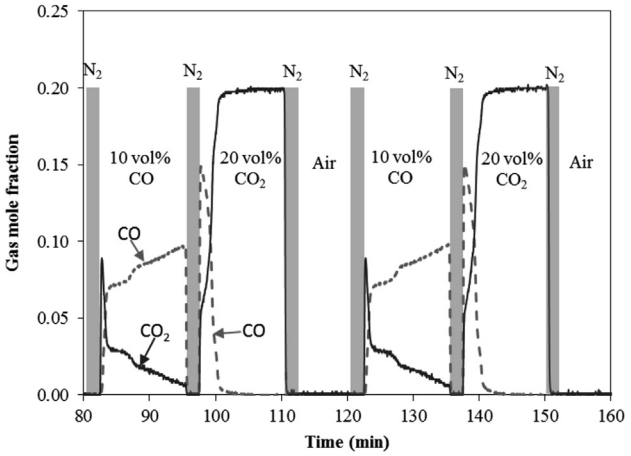

Fig. 5 – Concentration profile of the off gases during the 3rd and 4th cycles during the cycling experiment of FC57 particles in a fluidised bed at 1123 K. The periods with N_2 purge are indicated by the bars in grey.

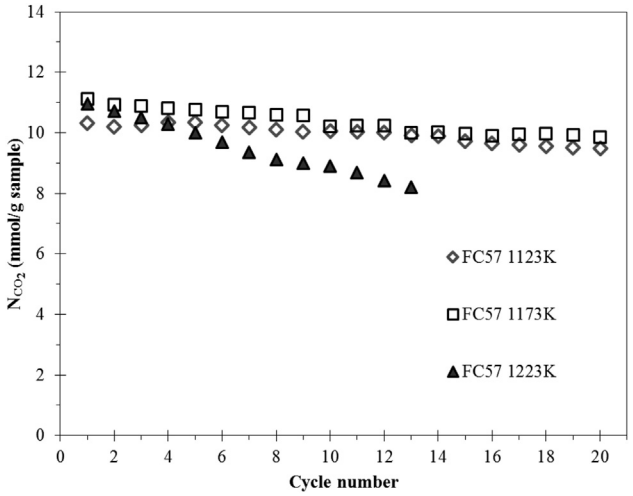

Fig. 7 – Yield of CO_2 produced by FC57 in each cycle during reduction at 1123 K–1223 K in fluidised bed.

1173 K, for FC0, FC50, FC57 and FC67 is shown in Fig. 8. For FC0, 95% of Fe_2O_3 is reduced to Fe during the 1st cycle, but the change in conversion, ΔX_{ox}, on the subsequent oxidation was only 24.2%; i.e. the material was unable to reoxidise during the 40 min oxidation. After the 1st cycle, the change in conversion during oxidation is similar to the change in conversion on reduction in the subsequent cycle, indicating that all of the material which is reoxidised can be subsequently reduced; i.e. the material is heavily sintered with reaction only taking place on any remaining iron oxide which is easily accessible by the reacting gases. In contrast, the addition of 50–66.7 mol% of CaO to Fe_2O_3 stabilised the performance. A gradual decrease in ΔX, a measure of the oxygen-carrying capacity, was found for all the CaO doped particles but the decrease was much slower than for FC0.

Using the overall yield or solid conversion as a measure of performance can be misleading, since if left long enough a 100% yield would be achieved. Therefore, it is useful to look how the variation of conversion with time changes over cycling, as in Fig. 9(a) and (b) for FC57 which shows that the material is very deeply reduced in the first cycle, and is able to fully reoxidise for the first 20 or so cycles. Large changes in behaviour are seen in the oxidation curves, which showed a significant slowdown in the kinetics. In contrast, Fig. 9(c) and (d) show the results from shorter cycles, in which the material is less reduced, with the kinetics during oxidation changing less drastically.

The ultimate conversion achieved in the first cycle in the fluidised bed at 1173 K (~88%, shown in Fig. 7) is less than that achieved in the TGA with longer cycling times (Fig. 8(a)) but is

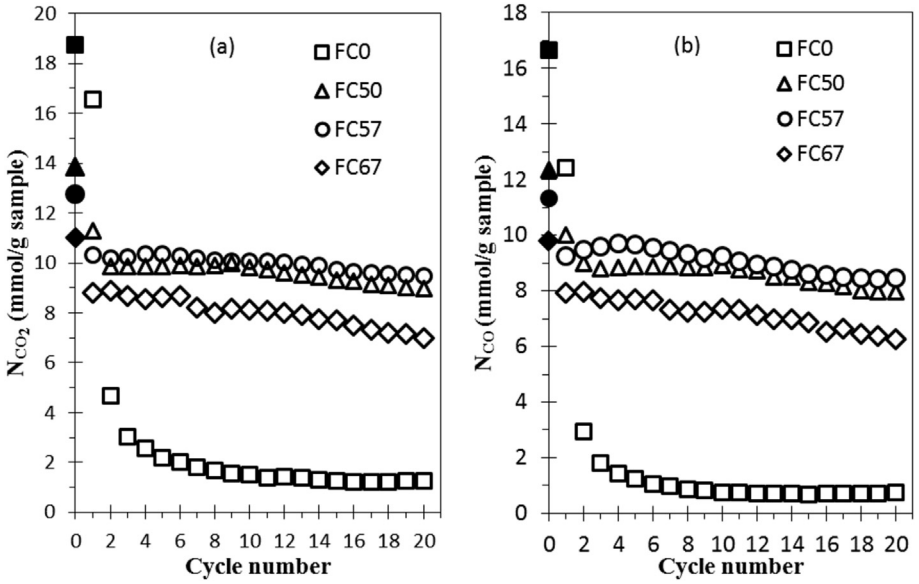

Fig. 6 – (a) Yield of CO_2 during reduction and (b) CO produced during CO_2-oxidation at 1123 K in the fluidised bed. The filled symbols on Y-axis show the expected amounts of CO_2 or CO if the respective material is fully reduced ($Fe^{3+} \rightarrow Fe$), then fully oxidised to the equivalent of Fe_3O_4 ($Fe \rightarrow Fe^{3+} + Fe^{2+}$).

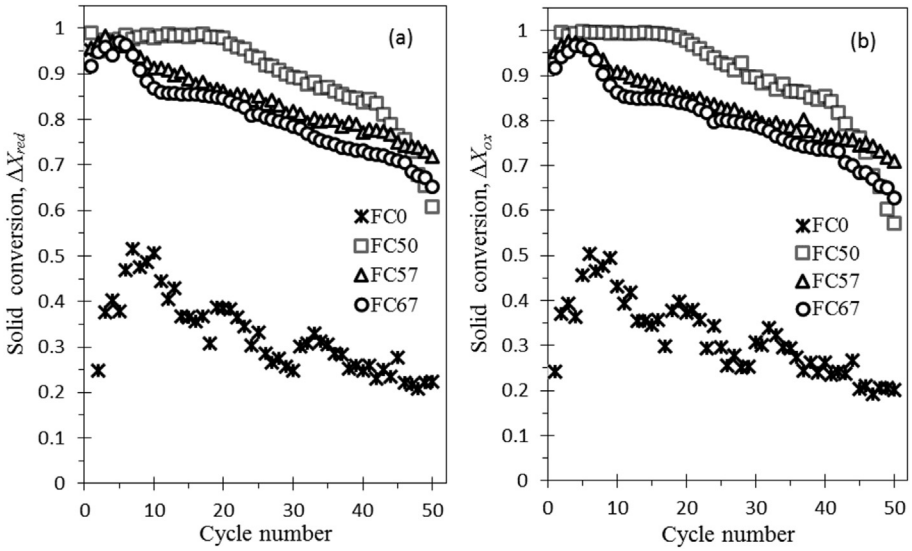

Fig. 8 – Change in solid conversion during (a) reduction with 5% H_2 and (b) oxidation with air, as function of cycle number in the TGA at 1173 K.

still significantly higher than that achieved in the TGA with shorter cycling times. Whilst there are differences in the experimental set up which might explain the different yields, notably the use of 10 mol% CO and the much reduced mass transfer resistance in the fluidised bed, this does suggest that higher degrees of reduction result in a faster decay of performance, but that a relatively high degree of reduction can be achieved without a drastic slowdown in kinetics.

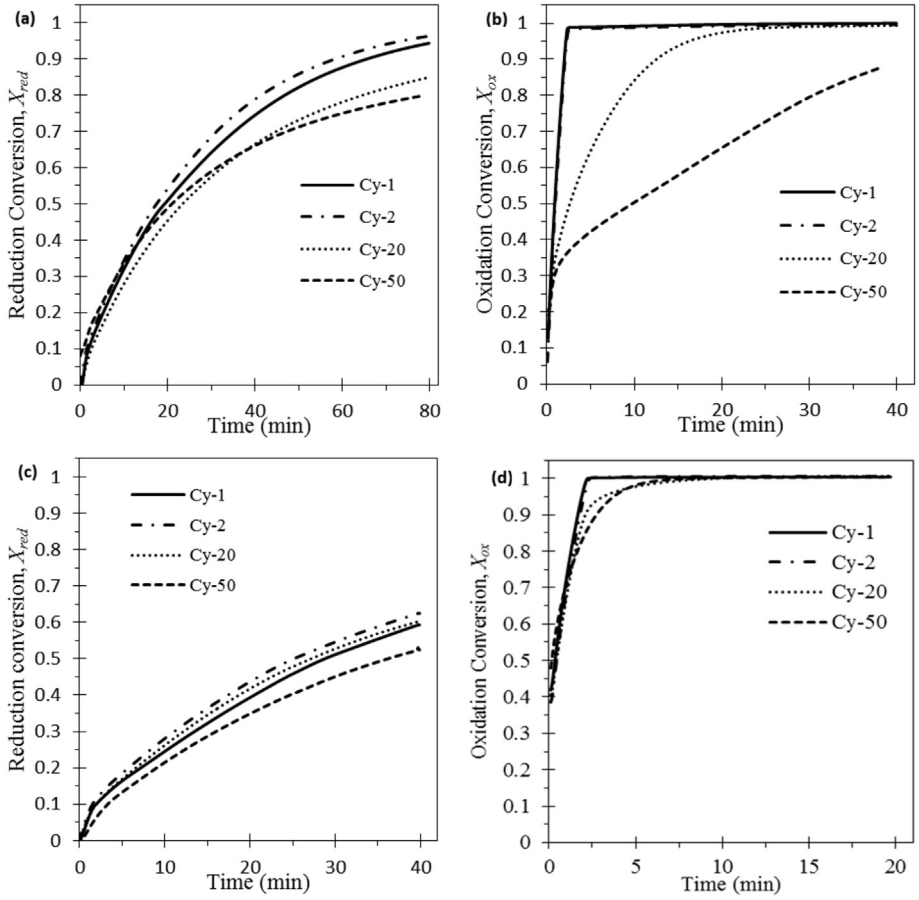

Fig. 9 – Conversion as a function of time for 50 cycles of oxidation and reduction of FC57 in the TGA at 1173 K. (a) and (b) show cycles for an experiment in which the material was reduced for 80 min using 5% H_2 (i.e. (a)) and oxidised using air for 40 min (i.e. (b)). (c) and (d) show a comparable experiment in which the reduction time was 40 min and the oxidation time was 20 min.

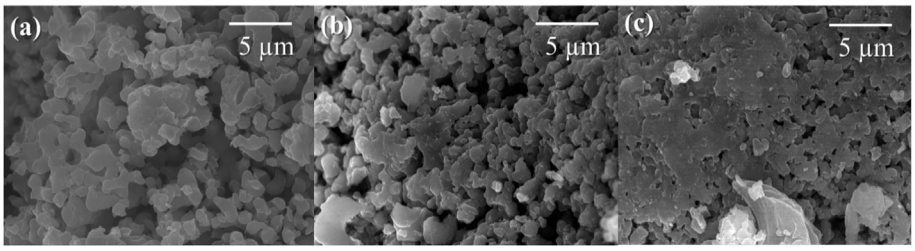

Fig. 10 – SEM images of external surface of FC57 when it is (a) freshly prepared, (b) air-oxidised after 10 cycles and (c) air-oxidised after 20 cycles at 1123 K in a fluidised bed.

Characterisation the oxygen carriers after cycling in a fluidised bed

SEM images of the FC57, when freshly-calcined, oxidised in air after 10 cycles and oxidised in air after 20 cycles (from the experiment in Fig. 6) are shown in Fig. 10. There does not appear to be a significant change in surface morphology after 10 cycles, but after the 20th cycle the surface appeared to have sintered; although some large pores are still visible. The BET areas measured for these materials were found to be small (~1 m^2/g) and thus at the detection limit of the instrument. After 10 cycles in the fluidised bed, the BET area of FC0 had fallen from 0.9 m^2/g to 0.1 m^2/g (to within the error of the instrument), whilst that for FC57 started at 1.1 m^2/g and was approximately the same (0.8 m^2/g) after 20 cycles. In contrast to FC0, no agglomeration was observed for the particles of FC57 recovered after the fluidised bed experiment.

The XRD patterns of the FC57 recovered after cycling are shown in Fig. 11. A number of peaks for Fe_2O_3, $CaFe_2O_4$ and $Ca_2Fe_2O_5$ overlap, making the patterns in Fig. 11 difficult to interpret by inspection, though there does appear to be a decrease in the intensity of peaks associated with $CaFe_2O_4$. Fig. 12 shows the result of a more rigorous approach, quantitative phase analysis using Rietveld refinement, and indicates a net decrease in the amount of $CaFe_2O_4$ and accompanying increases in the amounts of $Ca_2Fe_2O_5$ and Fe_2O_3 in the fully oxidised samples after cycling.

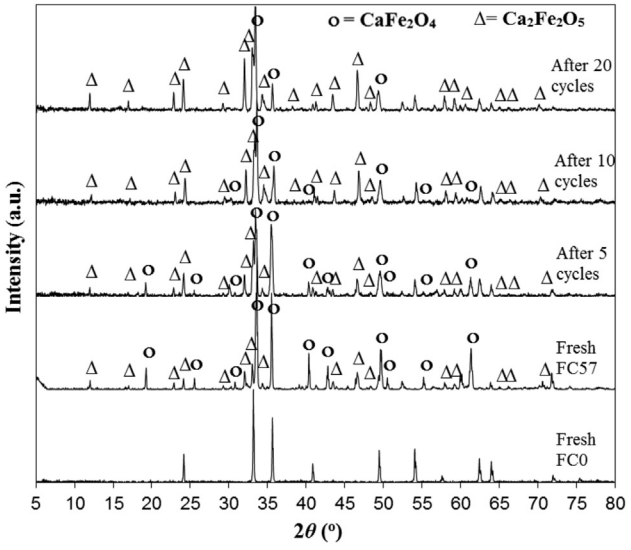

Fig. 11 – XRD patterns of FC57 and FC0 when fresh, and FC57 after 5, 10 and 20 cycles, air-oxidised. The cycling experiments were performed in fluidised beds at 1123 K. The unique peaks of $Ca_2Fe_2O_5$ and $CaFe_2O_4$ peaks are labelled by 'Δ' and 'o', respectively. The pattern for the fresh FC0 matches that of pure Fe_2O_3.

Reduction of the oxygen carriers with a high background concentration of CO_2

Since the addition of calcium and the resulting formation of ferrites alters the equilibrium oxygen fugacity for the phase transitions, some experiments were conducted with $\log(p_{O_2}) = \sim -14.1$, to examine the effect of calcium on the phase transitions which could be used for complete combustion.

In Fig. 13, FC0 behaved as expected with an ultimate conversion in line with reduction to Fe_3O_4. FC57 should reduce to $Ca_2Fe_2O_5 + CW_3F$ (according to Fig. 1) with a theoretical mass loss of 1.35% and a final $\Delta X_{red} = 0.055$ (assuming equilibrium phase composition to start with, i.e. 60 wt% $CaFe_2O_4$ + 40 wt% $Ca_2Fe_2O_5$); the $Ca_2Fe_2O_5$ should not be reduced. FC57 quickly reached an ultimate conversion slightly higher than that predicted. As shown in Table 1, the result of the XRD

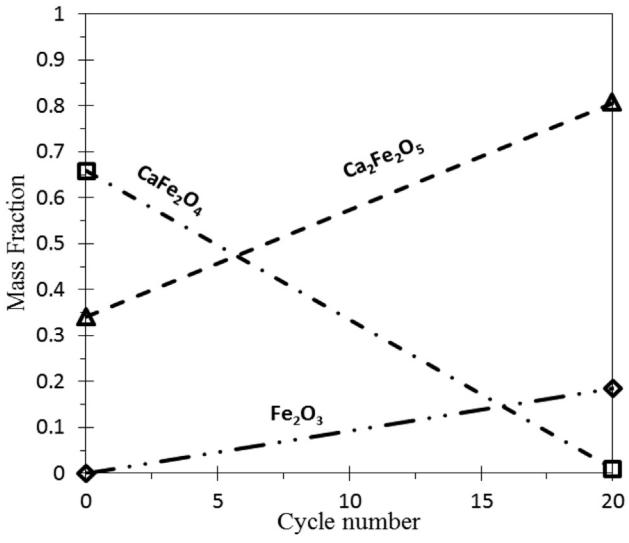

Fig. 12 – Mass fractions of the crystalline phases (obtained from Rietveld refinement of the XRD patterns) present in FC57 before and after cycling in a fluidised bed at 1123 K.

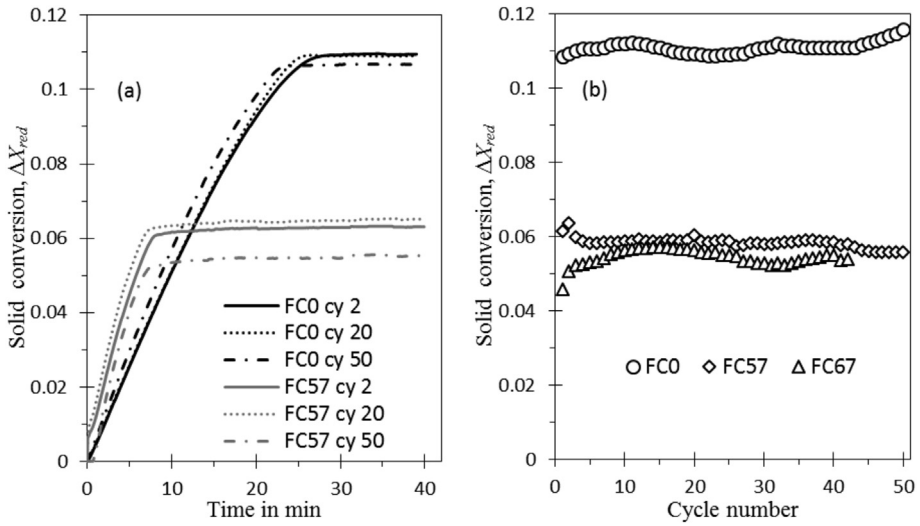

Fig. 13 – (a) Solid conversion during reduction with $\log(p_{O_2}) = \sim -14.1$ at 1173 K in the TGA. (b) Conversion as a function of cycle numbers during reduction. Reduction with a mixture of 50 vol% CO_2 + 5 vol% CO for 40 min, oxidation with air for 20 min.

refinement indicates the fresh material contains slightly more $CaFe_2O_4$ than anticipated (~66 wt% c.f. 60 wt%). This discrepancy has little effect on the overall oxygen transfer capacity, but gives a noticeable change in the amount of oxygen released during reduction to $Ca_2Fe_2O_5$ + CW_3F, and would suggest an anticipated ΔX_{red} of ~0.058. The ultimate conversion remains fairly constant with cycling, suggesting that the $CaFe_2O_4$ content of the particles remains fairly stable (in contrast to the observations in Fig. 12). FC67 (which at equilibrium should be entirely $Ca_2Fe_2O_5$) should not reduce, yet some change of mass is observed. Rietveld refinement showed that fresh FC67 contained ~40 wt% $CaFe_2O_4$ (in addition to a small amount of free Fe_2O_3), which could be reduced under these conditions. Again it is noteworthy that the oxygen carrier did not appear to approach its predicted equilibrium composition (i.e. 100% $Ca_2Fe_2O_5$) after many cycles.

Discussion

XRD of the fresh oxygen carriers shows the composition of most of the oxygen carriers did not reach the equilibrium composition expected for the Ca–Fe–O system during their initial calcination. For example, FC67 should only form $Ca_2Fe_2O_5$, yet its XRD pattern shows peaks of $Ca_2Fe_2O_5$, $CaFe_2O_4$ and CaO. The presence of several phases in FC67 is also reflected by the results of TPR (shown in Fig. 4) which indicates several stages of reduction as opposed to a single phase transition, $Ca_2Fe_2O_5 \rightarrow 2Fe + 2CaO + 1.5O_2$, expected from Fig. 1. Since the equilibrium p_{O_2} for $Ca_2Fe_2O_5 \rightarrow Fe + CaO$ is low, $Ca_2Fe_2O_5$ would be expected to be the last phase to reduce. Therefore, the broad peak on the DTG curves in Fig. 4 above ~1073 K for the FC67 material is likely to be the reduction of $Ca_2Fe_2O_5$. FC57 has a composition closer to the expected equilibrium initially, consisting of a mixture of $Ca_2Fe_2O_5$ and $CaFe_2O_4$. The reduction of the $CaFe_2O_4$ phase should undergo the steps tabulated in Table 2, assuming these steps take place in order of decreasing p_{O_2}.

It should be noted that above ~1143 K an additional reaction may take place between steps (R4) and (R5), in which the $CaFe_5O_7$ reduces to a halite phase containing CaO and FeO mixed with some $Ca_2Fe_2O_5$. The $Ca_2Fe_2O_5$ should remain unreacted whilst a sequence of reactions reduces the iron content in the $CaFe_2O_4$ fraction, producing additional

Table 2 – Reactions of mono-calcium ferrite ($CaFe_2O_4$) during reduction and associated equilibrium gas concentrations at 1123 K.

Reaction		Expected mass loss for FC57[a]	Equilibrium[c]	
			$Log_{10}(P_{O_2})$	$Log_{10}(P_{H_2}/P_{H_2O})$
$5CaFe_2O_4 \rightarrow 0.5Ca_2Fe_2O_5 + Ca_4Fe_9O_{17} + 0.25O_2$	(R2)	0.45%	−8.60	−4.35
$Ca_4Fe_9O_{17} \rightarrow 0.75Ca_2Fe_2O_5 + 2.5CaFe_3O_5 + 0.375O_2$	(R3)	0.67%	−14.90	−1.20
$CaFe_3O_5 \rightarrow 0.25Ca_2Fe_2O_5 + 0.5CaFe_5O_7 + 0.125O_2$	(R4)	0.56%	−16.94	−0.18
$CaFe_5O_7 \rightarrow 0.5Ca_2Fe_2O_5 + 4Fe + 2.25O_2$	(R5)	5.1%	−17.82	0.26
$Ca_2Fe_2O_5 \rightarrow 2Fe + 2CaO + 1.5O_2$	(R1)	6.74% + 6.95%[b]	−18.25	0.48

[a] Based on the equilibrium composition of $CaFe_2O_4$ and $Ca_2Fe_2O_5$.
[b] Additional mass lost from the reduction of $Ca_2Fe_2O_5$ originally in the sample.
[c] Equilibrium partial pressures in bar, computed from MTDATA using NPL oxide database (P_{O_2}) and the Scientific Group Thermodata Europe (SGTE) database (for conversion to P_{H_2}/P_{H_2O}) [42].

$Ca_2Fe_2O_5$; once the sample contains only $Ca_2Fe_2O_5$, this fraction will then reduce to iron and CaO. Thus, the TPR might be expected to show 5 peaks in the DTG curves, each corresponding to the reactions in Table 2. In contrast, Fig. 14 (which re-plots the rate of mass loss in Fig. 4 for FC57, as a function of normalised mass) shows only 2 distinct peaks. The final reduction (at the lowest normalised mass) should correspond to $Ca_2Fe_2O_5$ reducing to Fe and appears to correspond well with the expected mass change labelled by the distance R1. It is difficult to distinguish R2, 3, 4 from R5 in Fig. 14, since the mass changes associated with R2 − 4 are small; it is therefore likely the peak which occurs initially is consists of R2, 3 and 4 overlapping with R5 (which is responsible for the majority of the peak).

The equilibrium p_{O_2} for the reactions in Table 2 provide an indication of how difficult each of the materials is to reduce, and also consequently how easily they re-oxidise. Thermodynamically, $Ca_2Fe_2O_5$ is a very stable compound and its formation has the consequence that any Fe_2O_3 held within it is effectively inert for reactions used for chemical looping combustion. On the other-hand, this implies that it is beneficial for H_2 production and will readily react with H_2O to produce H_2. In fact, only R2 has a sufficiently high equilibrium p_{O_2} to be of use for CLC. Adding calcium therefore reduces the capacity of the material for combustion (for comparison the Fe_2O_3 to Fe_3O_4 transition usually used for CLC results in a mass change of 3.34 wt%), but increases the amount of oxygen available for hydrogen producing reactions. The equilibrium value of p_{H_2}/p_{H_2O} for the oxidation of the metallic iron back to the $Ca_2Fe_2O_5$ is higher than for iron to wüstite, (e.g. p_{H_2}/p_{H_2O} ~3 from Table 2 c.f. 1.7 for FeO/Fe at 1123 K) meaning less steam would have to be produced for generating hydrogen. Despite the fact that strong reducing conditions are needed to reduce the $Ca_2Fe_2O_5$, the kinetics of reduction are reasonable. This can be seen from the fluidised bed results in Fig. 6, where in the absence of a thermodynamic constraint, the particles gave high and stable conversions within 13 min, in contrast to the unmodified FC0. The phase diagram also suggests that it should be possible to reform $Ca_2Fe_2O_5$ by oxidation with CO_2.

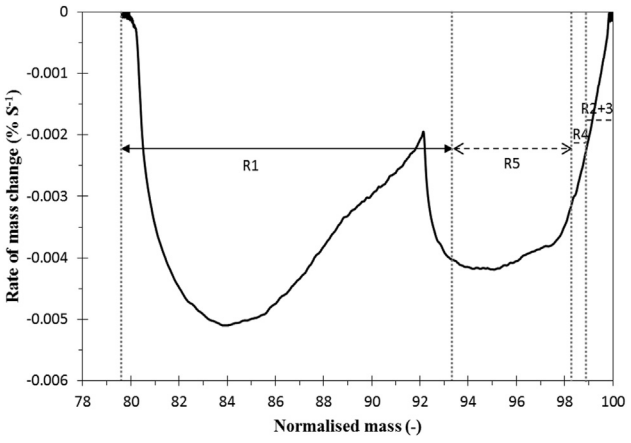

Fig. 14 − Plot of rate of mass change against normalised mass for fresh FC57 during TPR in H_2. Also shown are the mass changes expected from the reactions shown in Table 2.

All of the calcium containing materials presented here performed better over multiple redox cycles than the unmodified iron oxide, even when deeply reduced. The unsupported FC0, when reduced as deeply as the calcium containing materials, deactivated quickly and resulted in a completely sintered and unreactive particle. For the FC57 material, macro-porosity was still visible under the SEM after 20 cycles in the fluidised bed. Very deep reduction of the FC57 material, as in the TGA experiments shown in Fig. 8(a) and (b), did result in some noticeable deactivation, which is reflected by the reduced the rates of oxidation. This contrasts with the results of the fluidised bed experiments shown in Fig. 7, which showed little deactivation at 1173 K, where the material was reduced to a lesser extent. Whether or not it is the degree of reduction, or the time for which the material is held in the reduced state that promotes the deactivation (the TGA experiments were longer) requires further investigation. During reduction, almost all $CaFe_2O_4$, together with a significant fraction of the $Ca_2Fe_2O_5$ were reduced. Ferrite phases were able to reform during the oxidation, despite the formation of small amounts of free Fe_2O_3. Thus, the iron produced as a separate phase during reduction is mostly incorporated back into the ferrite phases during oxidation. Cycling of FC57, under conditions in which the $Ca_2Fe_2O_5$ could be reduced to Fe + CaO, increased the amount of $Ca_2Fe_2O_5$ (and Fe_2O_3) present, with very little $CaFe_2O_4$ left after 20 cycles at 1123 K, suggesting that cycling promotes segregation of phases within the oxygen carrier particles. In contrast, when reduction was limited by a high background level of CO_2, there appeared to be little change in the relative amounts of the mono and di-calcium ferrite, suggesting that compositional deviation from equilibrium and the segregation depends on how the particles are treated over a cycle. It would appear as if the $CaFe_2O_4$ will reform on oxidation, providing that the $Ca_2Fe_2O_5$ it produces is not reduced to Fe and CaO.

Reducing to Fe + CaO might cause some local segregation. $Ca_2Fe_2O_5$ can form at lower p_{O_2} values than other ferrite phases, so it is reasonable to assume that it forms first on re-oxidation, leaving iron rich phases. Locally $Ca_2Fe_2O_5$ can be stable in contact with other ferrite phases formed by oxidation and the conversion of the $Ca_2Fe_2O_5$ (calcium rich phase) to the other ferrites would require migration of Fe^{3+}, which may be a comparatively slow process, perhaps explaining the kinetic stability of the $Ca_2Fe_2O_5$.

In CLC, one of the major challenges for continuous operation in fluidised beds is agglomeration at higher temperatures. Cho et al. [49] found that agglomeration and defluidisation occurred very rapidly during cycling with iron oxides at a high temperature, particularly above 1223 K. They also found a deeper reduction of iron oxide (and the formation of wüstite) was associated with more severe agglomeration. In this work, when the particles were more deeply reduced as in the experiments shown in Fig. 6(a), in which a significant amounts of metallic iron were formed, the bed defluidised for FC0. In contrast, the CaO modified material did not show any significant agglomeration or defluidisation even after 20 cycles at 1123 K. At 1173 K some agglomeration was observed for FC50 whilst the OCs containing more calcium (FC57, FC67) did not show any agglomeration. At 1223 K all materials agglomerated to a certain extent.

During the fluidised bed experiments shown in Fig. 6, all the oxygen carrier particles experienced some attrition. Over the 13 h of cycling, ~9% of the FC0 was elutriated due to attrition (determined from the mass of material remaining in the bed), whereas for FC50, FC57, FC67 the loss was between 4 and 6 wt%. Mechanical strength would need to be improved for commercial application e.g. by pelletising or extrusion and spheronisation.

So far, the experimental results have demonstrated the potential of using mixtures of calcium ferrites as stable OCs for CLH. However, the accumulation of $Ca_2Fe_2O_5$, which is thermodynamically difficult to reduce, makes the OCs less competitive for CLC. To make these materials suitable for commercial operations, further development is necessary to improve the OCs' properties such as the resistance to attrition.

Conclusions

A simple mechanical mixing method was used to synthesise oxygen carriers from CaO and Fe_2O_3. The mixed oxides contained Ca-ferrites ($Ca_2Fe_2O_5$ and $CaFe_2O_4$). All the Ca-containing carriers were more stable during cycling than the unmodified iron oxide, and the calcium ferrites proved to be readily reducible and reformed upon re-oxidation. Significant deviations from the expected equilibrium phase compositions were observed in the oxidised material, and this was also influenced by cycles of oxidation and reaction, and how deeply the particles were reduced in a cycle: deep reduction of the materials appeared to promote the formation of $Ca_2Fe_2O_5$, even when the content of $Ca_2Fe_2O_5$ exceeded that expected to form at equilibrium. Although some sintering of the mixed oxide material was observed, its impact on the performance was limited and surface area and porosity sufficient for chemical looping reactions were maintained. Amongst the synthesised OCs the material containing 57.3 mol% CaO showed the best performance. However, the addition of large amounts of calcium oxide results in the carriers having less oxygen-carrying capacity for conventional CLC, but additional capacity for hydrogen production.

Data

All the supporting data for this work can be found on https://www.repository.cam.ac.uk.

Acknowledgements

The authors would like to thank Prof. Clare Grey for her invaluable help in the XRD analysis and Z. Saracevic for support in operating the gas adsorption analyser. This work was supported by the Engineering and Physical Sciences Research Council (EPSRC grant EP/I070912/1). The first author is grateful to IDB (Islamic Development Bank) – Cambridge International Scholarship body for financial support for PhD study. W. L acknowledges funding from the National Research Foundation (NRF), Prime Minister's Office, Singapore under its Campus for Research Excellence and Technological Enterprise (CREATE) programme.

REFERENCES

[1] Jin H, Ishida M. A new type of coal gas fueled chemical-looping combustion. Fuel 2004;83:2411–7. http://dx.doi.org/10.1016/j.fuel.2004.06.033.
[2] Rydén M, Leion H, Mattisson T, Lyngfelt A. Combined oxides as oxygen-carrier material for chemical-looping with oxygen uncoupling. Appl Energy 2014;113:1924–32. http://dx.doi.org/10.1016/j.apenergy.2013.06.016.
[3] Fang H, Haibin L, Zengli Z. Advancements in development of chemical-looping combustion: a review. Int J Chem Eng 2009;2009:1–16. http://dx.doi.org/10.1155/2009/710515.
[4] Jerndal E, Leion H, Axelsson L, Ekvall T, Hedberg M, Johansson K, et al. Using low-cost iron-based materials as oxygen carriers for chemical looping combustion. Oil Gas Sci Technol Rev IFP Energies Nouv 2011;66:235–48. http://dx.doi.org/10.2516/ogst/2010030.
[5] Xiao R, Song Q, Song M, Lu Z, Zhang S, Shen L. Pressurized chemical-looping combustion of coal with an iron ore-based oxygen carrier. Combust Flame 2010;157:1140–53. http://dx.doi.org/10.1016/j.combustflame.2010.01.007.
[6] Rydén M, Cleverstam E, Lyngfelt A, Mattisson T. Waste products from the steel industry with NiO as additive as oxygen carrier for chemical-looping combustion. Int J Greenh Gas Control 2009;3:693–703.
[7] Berguerand N, Lyngfelt A. Chemical-looping combustion of petroleum coke using ilmenite in a 10 kW th unit–high-temperature operation. Energy Fuels 2009;23:5257–68. http://dx.doi.org/10.1021/ef900464j.
[8] Bohn CD, Müller CR, Cleeton JP, Hayhurst AN, Davidson JF, Scott SA, et al. Production of very pure hydrogen with simultaneous capture of carbon dioxide using the redox reactions of iron oxides in packed beds. Ind Eng Chem Res 2008;47:7623–30.
[9] Bohn CD, Cleeton JP, Müller CR, Davidson JF, Hayhurst AN, Scott SA, et al. The kinetics of the reduction of iron oxide by carbon monoxide mixed with carbon dioxide. AIChE J 2010;56:1016–29. http://dx.doi.org/10.1002/aic.
[10] Thursfield A, Murugan A, Franca R, Metcalfe IS. Chemical looping and oxygen permeable ceramic membranes for hydrogen production – a review. Energy Environ Sci 2012;5:7421–59. http://dx.doi.org/10.1039/C2EE03470K.
[11] Galvita V, Schröder T, Munder B, Sundmacher K. Production of hydrogen with low COx-content for PEM fuel cells by cyclic water gas shift reactor. Int J Hydrogen Energy 2008;33:1354–60. http://dx.doi.org/10.1016/j.ijhydene.2007.12.022.
[12] Rydén M, Arjmand M. Continuous hydrogen production via the steam–iron reaction by chemical looping in a circulating fluidized-bed reactor. Int J Hydrogen Energy 2012;37:4843–54. http://dx.doi.org/10.1016/j.ijhydene.2011.12.037.
[13] Urasaki K, Tanimoto N, Hayashi T, Sekine Y, Kikuchi E, Matsukata M. Hydrogen production via steam–iron reaction using iron oxide modified with very small amounts of palladium and zirconia. Appl Catal A Gen 2005;288:143–8. http://dx.doi.org/10.1016/j.apcata.2005.04.023.
[14] Lorente E, Peña JA, Herguido J. Separation and storage of hydrogen by steam-iron process: effect of added metals upon hydrogen release and solid stability. J Power Sources 2009;192:224–9. http://dx.doi.org/10.1016/j.jpowsour.2008.12.116.
[15] Hacker V, Fankhauser R, Faleschini G, Fuchs H, Friedrich K, Muhr M, et al. Hydrogen production by steam–iron process. J

Power Sources 2000;86:531–5. http://dx.doi.org/10.1016/S0378-7753(99)00458-9.
[16] Gupta P, Velazquez-vargas LG, Fan L. Syngas redox (SGR) process to produce hydrogen from coal derived syngas. Energy Fuels 2007;21:2900–8.
[17] Svoboda K, Slowinski G, Rogut J, Baxter D. Thermodynamic possibilities and constraints for pure hydrogen production by iron based chemical looping process at lower temperatures. Energy Convers Manag 2007;48:3063–73. http://dx.doi.org/10.1016/j.enconman.2007.05.019.
[18] de Diego LF, Garcıa-Labiano F, Adánez J, Gayán P, Abad A, Corbella BM, et al. Development of Cu-based oxygen carriers for chemical-looping combustion. Fuel 2004;83:1749–57. http://dx.doi.org/10.1016/j.fuel.2004.03.003.
[19] Ishida M, Jin H. A novel chemical-looping combustor without NO_x formation. Ind Eng Chem Res 1996;35:2469–72.
[20] Johansson M, Mattisson T, Lyngfelt A. Investigation of Fe_2O_3 with $MgAl_2O_4$ for chemical-looping combustion. Ind Eng Chem Res 2004;43:6978–87.
[21] Zafar Q, Mattisson T, Gevert B. Redox investigation of some oxides of transition-state metals Ni, Cu, Fe, and Mn supported on SiO_2 and $MgAl_2O_4$. Energy Fuels 2006;20:34–44.
[22] Li F, Kim HR, Sridhar D, Zeng L, Chen J, Fan L, et al. Syngas chemical looping gasification process: oxygen carrier particle selection and performance. Energy Fuels 2009;23:4182–9. http://dx.doi.org/10.1021/ef900236x.
[23] Kierzkowska AM, Bohn CD, Scott SA, Cleeton JP, Dennis JS, Müller CR. Development of iron oxide carriers for chemical looping combustion using sol-gel. Ind Eng Chem Res 2010;49:5383–91.
[24] Bohn CD, Cleeton JP, Müller CR, Chuang SY, Scott SA, Dennis JS. Stabilizing iron oxide used in cycles of reduction and oxidation for hydrogen production. Energy Fuels 2010;24:4025–33. http://dx.doi.org/10.1021/ef100199f.
[25] Galvita V, Sundmacher K. Redox behavior and reduction mechanism of Fe_2O_3–$CeZrO_2$ as oxygen storage material. J Mater Sci 2007;42:9300–7. http://dx.doi.org/10.1007/s10853-007-1872-7.
[26] Liu W, Dennis JS, Scott SA. The effect of addition of ZrO_2 to Fe_2O_3 for hydrogen production by chemical looping. Ind Eng Chem Res 2012;51:16597–609. http://dx.doi.org/10.1021/ie302626x.
[27] Liu W, Ismail M, Dunstan MT, Hu W, Zhang Z, Fennell PS, et al. Inhibiting the interaction between FeO and Al_2O_3 during chemical looping production of hydrogen. RSC Adv 2014;5:1759–71. http://dx.doi.org/10.1039/C4RA11891J.
[28] Kidambi PR, Cleeton JPE, Scott SA, Dennis JS, Bohn CD. Interaction of iron oxide with alumina in a composite oxygen carrier during the production of hydrogen by chemical looping. Energy Fuels 2012;26:603–17. http://dx.doi.org/10.1021/ef200859d.
[29] Knutsson P, Linderholm C. Characterization of ilmenite used as oxygen carrier in a 100 kW chemical-looping combustor for solid fuels. Appl Energy 2015;157:368–73. http://dx.doi.org/10.1016/j.apenergy.2015.05.122.
[30] Abad A, Adánez J, Cuadrat A, García-Labiano F, Gayán P, de Diego LF. Kinetics of redox reactions of ilmenite for chemical-looping combustion. Chem Eng Sci 2011;66:689–702. http://dx.doi.org/10.1016/j.ces.2010.11.010.
[31] Li F, Luo S, Sun Z, Bao X, Fan L-S. Role of metal oxide support in redox reactions of iron oxide for chemical looping applications: experiments and density functional theory calculations. Energy Environ Sci 2011;4:3661–7. http://dx.doi.org/10.1039/C1EE01325D.
[32] Svoboda K, Siewiorek A, Baxter D, Rogut J, Punčochář M. Thermodynamic possibilities and constraints of pure hydrogen production by a chromium, nickel, and manganese-based chemical looping process at lower temperatures. Chem Pap 2007;61:110–20. http://dx.doi.org/10.2478/s11696-007-0007-6.
[33] Aston VJ, Evanko BW, Weimer AW. Investigation of novel mixed metal ferrites for pure H_2 and CO_2 production using chemical looping. Int J Hydrogen Energy 2013;38:9085–96. http://dx.doi.org/10.1016/j.ijhydene.2013.05.078.
[34] Murugan A, Thursfield A, Metcalfe IS. A chemical looping process for hydrogen production using iron-containing perovskites. Energy Environ Sci 2011;4:4639–49. http://dx.doi.org/10.1039/C1EE02142G.
[35] Dueso C, Thompson C, Metcalfe I. High-stability, high-capacity oxygen carriers: iron oxide-perovskite composite materials for hydrogen production by chemical looping. Appl Energy 2015;157:382–90. http://dx.doi.org/10.1016/j.apenergy.2015.05.062.
[36] Li F, Sun Z, Luo S, Fan L-S. Ionic diffusion in the oxidation of iron – effect of support and its implications to chemical looping applications. Energy Environ Sci 2011;4:876–80. http://dx.doi.org/10.1039/C0EE00589D.
[37] Hillert M, Selleby M, Sundman B. An assessment of the Ca–Fe–O system. Metall Trans A 1990;21:2759–76. http://dx.doi.org/10.1007/BF02646071.
[38] Shaula AL, Markov AA, Naumovich EN, Waerenborgh JC, Pivak YV, Kharton VV. Redox behavior and transport properties of brownmillerite $Ca_2(Fe,M)_2O_{5\pm\delta}$ (M = Mn, Co). Solid State Ion 2012;225:206–10. http://dx.doi.org/10.1016/j.ssi.2011.11.016.
[39] Lee SJ, Yong S-M, Kim DS, Kim DK. Cobalt-free composite cathode for SOFCs: brownmillerite-type calcium ferrite and gadolinium-doped ceria. Int J Hydrogen Energy 2012;37:17217–24. http://dx.doi.org/10.1016/j.ijhydene.2012.08.100.
[40] Hirabayashi D, Yoshikawa T, Mochizuki K, Suzuki K, Sakai Y. Formation of brownmillerite type calcium ferrite ($Ca_2Fe_2O_5$) and catalytic properties in propylene combustion. Catal Lett 2006;110:269–74. http://dx.doi.org/10.1007/s10562-006-0120-0.
[41] Il'in AP, Smirnov NN, Il'in AA. Mechanochemical synthesis of calcium and copper ferrite catalysts for medium-temperature carbon monoxide conversion. Kinet Catal 2006;47:901–6. http://dx.doi.org/10.1134/S0023158406060139.
[42] Davies RH, Dinsdale AT, Gisby JA, Robinson JAJ, Martin SM. MTDATA - Thermodynamic and phase equilibrium software from the national physical laboratory. Calphad 2002;26(2):229–71.
[43] Wen C, Yu Y. A generalized method for predicting the minimum fluidization velocity. AIChE J 2004;12:610–2.
[44] Larson AC, Dreele Von RB. GSAS: the general structure analysis program. NM, USA: Los Alamos Natl Lab Los Alamos; 1990.
[45] Toby BH. EXPGUI, a graphical user interface for GSAS. J Appl Crystallogr 2001;34:210–3. http://dx.doi.org/10.1107/S0021889801002242.
[46] Brunauer S, Emmett P, Teller E. Adsorption of gases in multimolecular layers. J Am Chem Soc 1938;60:309–19.
[47] Liu W, Dennis JS, Scott SA. The effect of addition of ZrO_2 to Fe_2O_3 for hydrogen production by chemical looping. Ind Eng Chem Res 2012;51:16597–609.
[48] Bohn CD. The production of pure hydrogen with simultaneous capture of carbon dioxide. UK: University of Cambridge; 2010. PhD thesis.
[49] Cho P, Mattisson T, Lyngfelt A. Defluidization conditions for a fluidized bed of iron oxide-, nickel oxide-, and manganese oxide-containing oxygen carriers for chemical-looping combustion. Ind Eng Chem Res 2006;45:968–77. http://dx.doi.org/10.1021/ie050484d.